NATIONAL ADVISORY COMMITTEE FOR AERONAUTICS

TECHNICAL NOTE

No. 1657

EFFECTS OF COMPRESSIBILITY ON THE FLOW PAST THICK AIRFOIL SECTIONS

By Bernard N. Daley and Milton D. Humphreys

Langley Aeronautical Laboratory
Langley Field, Va.

Washington

July 1948

NATIONAL ADVISORY COMMITTEE FOR AERONAUTICS

TECHNICAL NOTE NO. 1657

EFFECTS OF COMPRESSIBILITY ON THE FLOW PAST THICK AIRFOIL SECTIONS

By Bernard N. Daley and Milton D. Humphreys

SUMMARY

Six, 3-inch-chord symmetrical airfoil sections having systematic variations in thickness and maximum-thickness location were tested at Mach numbers near flight values for propeller-shank sections. The tests, the results of which are presented in the form of schlieren photographs of the flow past each model and pressure-distribution charts for two of the models, were performed to illustrate the effects of compressibility on the flow past thick symmetrical airfoil sections. Representative flow photographs indicated that at Mach numbers approximately 0.05 above the critical Mach number a speed region was reached in which the flow oscillated rapidly and the separation point and the location of the shock wave were unstable. Fixing the transition on both surfaces of the airfoil was effective in reducing these rapid oscillations. The pressure distributions showed that the section normal-force coefficients for thick airfoils were very erratic at subcritical speeds; at supercritical speeds the section normal-force coefficients for the thick airfoils became more regular. Drag coefficients showed that considerable drag decreases can be expected by decreasing the model thickness ratio.

INTRODUCTION

The rotational speed of the propeller has been limited heretofore by the compressibility losses at the blade tips, but as a consequence of the development of higher speed aircraft the thicker root sections can exceed their critical speeds and therefore serious adverse effects can be expected near the shanks. The purpose of this investigation was to illustrate the effects of compressibility on thick symmetrical airfoils suitable for use as propeller-shank sections. By utilizing pressure-distribution data and schlieren photographs of the air flow, force characteristics and information concerning the flow phenomena have been obtained. Test results for systematic variations of the maximum thickness-to-chord ratios, as well as results for variation of the chordwise location of maximum thickness, are included herein.

SYMBOLS

c_d	section drag coefficient
c_l	section lift coefficient
c_n	section normal-force coefficient
P	pressure coefficient
P_{cr}	critical-pressure coefficient
M	Mach number
M_{ch}	choking Mach number
M_{cr}	critical Mach number
q	stream dynamic pressure
α	angle of attack

APPARATUS, MODELS, AND TESTS

Tunnel.- The tests were made in the Langley rectangular high-speed tunnel. The tunnel (fig. 1) is of the closed-throat, nonreturn, induction type, utilizing air at high pressure in an annular nozzle located downstream from the test section to induce a flow of air from the atmosphere through the tunnel. The height of the test section is 18 inches and the width is 4 inches. The 4-inch walls are flexible; adjustments of the contours of these walls produce variations of the longitudinal static-pressure gradient of the tunnel. For these tests the wall settings were such as to maintain uniform pressure throughout the test section without a model at any Mach number below 0.85. The airfoils completely spanned the 4-inch dimension of the tunnel and were supported in such a manner that no external interference to either the air flow or to the optical field was possible.

Models.- The airfoil models investigated had 3-inch chords and were as follows:

Airfoil section	Maximum-thickness location (percent chord)	Leading-edge radius	Reference
NACA 0040-63	30	Normal	1
NACA 0040-64	40	Normal	1
NACA 0040-65	50	Normal	1
NACA 16-040	50	0.444 × Normal	2
NACA 16-025	50	.444 × Normal	2
NACA 16-015	50	.444 × Normal	2

The airfoil profiles are presented in figure 2.

Optical equipment.- The optical equipment used in these tests (fig. 1) is similar to that described in reference 3. Changes in the index of refraction of the air associated with changes in air density are made visible with this apparatus. Compression shock waves and separation phenomena, as well as generalized regions of density change, are shown on the photographs as regions of various degrees of light.

Tests.- Photographs of the flow around the airfoil models at zero angle of attack were made by means of the schlieren method at all attainable supercritical speeds. Supplemental schlieren tests were made of the NACA 0040-65 airfoil to determine the effects of fixing transition at the quarter-chord location. (See figs. 3 to 10.) High-speed motion pictures of the flow were also made by means of the schlieren method of air-flow photography (fig. 11). Data obtained from these schlieren tests are presented in figure 12. Pressure-distribution data for the NACA 16-040 and the NACA 16-025 airfoils were obtained at angles of attack from -2° to 12°. (See figs. 13 to 16.) Integrations of the pressure-distribution plots provided normal-force and pressure-drag coefficients for these models. The approximate Mach number range was from 0.33 to 0.73 for the 40-percent-thick airfoil models, from 0.33 to 0.78 for the 25-percent-thick airfoil model, and from 0.33 to 0.85 for the 15-percent-thick airfoil model. These Mach number ranges are comparable to those encountered in flight. The high-speed range was limited by the choking speed of the tunnel (reference 4). Air-stream Mach number was determined by the pressure measured at a calibrated static-pressure orifice upstream of the test section. The Reynolds number range for these tests was from 550,000 to 1,050,000.

PRECISION

Constriction of the flow field of the model by the tunnel walls (references 4 and 5) subjects the data to the largest source of error. Since constriction corrections are of questionable applicability at supercritical speeds, no constriction corrections have been applied to

these data. In order to give an indication of the magnitude of the correction for model blockage or constriction, however, some corrections have been calculated by the method of Allen and Vincenti (reference 5). Although these values vary to some extent with model thickness ratio and Mach number, the following table indicates the approximate value of the correction at all subcritical speeds:

NACA 16-040 airfoil	NACA 16-015 and 16-115 airfoils
Corrected $c_n = 0.965c_n$	Corrected $c_n = 0.975c_n$
Corrected $c_d = 0.965c_d$	Corrected $c_d = 0.985c_d$
Corrected $M = 1.015M$	Corrected $M = 1.010M$
Corrected $q = 1.025q$	Corrected $q = 1.015q$

Other errors due to velocity fluctuations, air-stream alinement, tunnel calibrations, and tunnel gradients (without model) are appreciably less than the constriction errors and thus for practical purposes are believed to be negligible. Serious humidity effects are not expected because all data in the present paper were obtained when the atmospheric relative humidity was below a value previously determined by a special investigation to be satisfactory.

The pressure-distribution diagrams and the schlieren photographs are presented for Mach numbers approaching the choking Mach number of the tunnel; the basic data for section normal-force and pressure-drag coefficients (figs. 17, 18, 22, and 23) are presented for Mach numbers up to the choking condition. The normal-force curves (figs. 17 and 18) are dashed within 0.04 of the choking Mach number. In this range the normal-force and drag data can reasonably be assumed to be affected by the choked condition. In the cross plots (figs. 19 to 21) data within this 0.04 range of Mach number are omitted.

RESULTS AND DISCUSSION

Flow Characteristics

Schlieren photographs of the flow field of the models (figs. 3 to 10) were made to show the effect on the air flow caused by variation of two fundamental design parameters of airfoils - the maximum thickness and the maximum-thickness location. These data indicated the probability of a rapidly oscillating flow in the supercritical speed range of these tests. In order to substantiate the existence of high-frequency oscillations occurring in the flow in this speed range, high-speed motion pictures of the flow past

thick airfoils at constant Mach numbers were made by means of the schlieren method. A representative strip of this movie film (fig. 11) shows a flow of irregular nature in which the angle of departure of the wake, the position of the point of separation, and the positions of the shock waves vary at high frequency.

From a consideration of the schlieren photographs, with the exception of the flow about models with fixed transition (figs. 6 and 7), three general flow types are encountered in the supercritical speed region:

(1) A semistable, moderately separated flow in which the separation points of both surfaces exhibit an erratic and persistent dissymmetry of position over a speed range extending from some subcritical Mach number to a value approximately 0.05 above the critical Mach number M_{cr} (figs. 5(a) and 8(a))

(2) A flow, in a higher supercritical speed range, characterized by relatively regular high-frequency oscillations of the wake, shock waves, and positions of the separation points (figs. 11 and 4(b) to 4(d))

(3) A relatively steady separated flow originating at speeds greater than those at which oscillating flow (type 2) is encountered and extending to the choking Mach number of the tunnel M_{ch}. The region for type 3 flow is quite narrow for the thicker airfoils of these tests and it is, therefore, difficult to distinguish between a true-flow type and the influence of the choked condition of the tunnel. The schlieren photographs for the NACA 16-015 airfoil (figs. 10(c) to 10(e)), however, offer good substantiation for this smooth flow at the higher supercritical speeds.

Figure 12 presents for each airfoil the boundaries of the various types of flow encountered at supercritical speeds. The data for this figure were obtained from a series of individual instantaneous schlieren photographs taken at random Mach numbers over the speed range. The curves for critical Mach number and the curves bounding the oscillating-flow region are therefore defined only by interpolation between exact test points; however, the curves may be considered as close approximations to the speeds at which these conditions exist.

Variation in maximum-thickness location.- The schlieren photographs (figs. 3 to 5) and the graph (fig. 12) indicate that for airfoils having constant thickness the rearward movement of the location of maximum thickness from 0.3- to 0.5-chord stations had the following effects: the value of the critical Mach number was increased from 0.51 to 0.58 and, consequently, the Mach number for shock formation was delayed by approximately the same amount; the Mach number for the onset of oscillating flow (type 2) was moved to a higher value without appreciably influencing the Mach number range of this type of flow (fig. 12); the violence of these fluctuations and the chordwise shifting of the separation point were reduced; the point of separation was moved rearward permitting a narrowing of the separated wake and the consequent indication of lower drag. These schlieren photographs (figs. 3 to 5) thus indicate that, in addition to the increase of critical Mach number shown also by previous work,

some slight improvement at supercritical speeds may be obtained by a rearward location of the point of maximum thickness.

Variation of maximum thickness.- The effects of decreasing the maximum thickness of the 16-series sections from 40 percent to 15 percent chord were to increase the value of the critical Mach number from 0.57 to 0.75, to delay the occurrence of oscillating flow (type 2) by a similar amount, and to move the separation point toward the trailing edge. It is apparent also from the schlieren photographs in figures 8 to 10 and from the data in figure 12 that a reduction in the thickness of the section decreased the Mach number range for oscillating flow (type 2) and reduced the violence of the wake fluctuations. It is further evidenced by a study of the data for the NACA 16-015 airfoil (figs. 10(c) to 10(e) and 12) that the extent of the Mach number range for type 3 flow is increased with a decrease in maximum thickness. A decrease in the thickness ratio is therefore the most effective method of delaying and minimizing the undesirable flow characteristics at supercritical Mach numbers.

Fixed transition.- In an effort to determine the effect of fixed transition on the flow, No. 60 carborundum grains were affixed along the span at the quarter-chord location on the NACA 0040-65 airfoil. This location was chosen because photographs of the flow past the smooth model indicated that this location was ahead of the most forward location of the separation point. Schlieren photographs are presented for the flow with fixed transition on the upper surface (fig. 6) and on both surfaces (fig. 7). At the lowest speeds the transition strips along the quarter-chord location seemed to produce an adverse effect on the wake width and the location of the separation point (compare figs. 5(a), 6(a), and 7(a)). In that speed range where oscillating flow (type 2) occurred for the smooth models, the oscillation of the wake, the movement of the separation point, and the movement of the shock waves have been effectively minimized by fixing transition (compare figs. 5 and 7). The flow at high Mach numbers appears to be improved considerably by fixing transition on both surfaces of the airfoil; fixing transition may produce good results in cases in which vibrations are a serious problem. At high Reynolds numbers or with airfoils having the transition point already far forward, the oscillations of the flow may be less severe than found in these experiments.

Airfoil Force Characteristics

Airfoil normal forces.- Figures 13 to 16 show variations of representative pressure distributions with Mach number for the NACA 16-025 and the NACA 16-040 airfoils. The data of figures 14(a), 14(b), and 16(a) to 16(d) indicate a pronounced variation with Mach number of the surface loading near the trailing edge of the model. This variation is caused at subcritical speeds by the semistable

unpredictable nature of the separation point characteristic of type 1 flow. (The critical-pressure coefficient P_{cr} is represented by the horizontal broken lines on the pressure-distribution charts.) These data indicate correspondingly large and unpredictable changes in section normal-force coefficients with Mach number. Such indications of changes in normal-force characteristics are confirmed by corresponding integrated section normal-force data of figures 17 and 18. The normal-force coefficients at subcritical and low supercritical speeds where erratic separated flow (type 1) predominates are generally irregular and these data probably cannot be reproduced accurately. Also as a result of assymetrical separation phenomena, the angle of attack for zero lift is considerably displaced. A similarly irregular zero-lift angle has been observed in data for the NACA 16-530 airfoil as tested in the Langley 24-inch high-speed tunnel (reference 2). Those unpredictable semistable normal-force characteristics (type 1 flow) exhibited by the thicker sections make the application of these airfoils to propeller-shank sections extremely undesirable and uncertain in this speed range.

As mentioned in the section entitled "Flow Characteristics," at Mach numbers approximately 0.05 above the critical, the flow becomes oscillating (type 2) and the separation point loses the former erratic and semistable nature of type 1 flow. This speed range corresponds closely to the speed at which the normal-force curves (figs. 17 and 18) first assume a regular variation with Mach number or angle of attack. In this Mach number range the angle of attack for zero lift approaches zero. All pressures that are recorded when the flow is oscillating rapidly are average pressures, and therefore the large flow variations that appear in the schlieren photographs in this speed range do not have a corresponding effect on the pressure data. The aforementioned phenomena are also clearly illustrated in figures 19 and 20, which present the variation of section normal-force coefficient with angle of attack for several Mach numbers. Lift data for the NACA 16-115 airfoil from the Langley 24-inch high-speed tunnel are presented in figure 21 for the purpose of illustrating the improvements that can be obtained by using thinner airfoil sections. A general improvement can be observed in the regularity of the lift-curve slope. The angle of attack for zero lift also does not vary in the Mach number range presented.

Airfoil drag characteristics.- The lack of pressure recovery at the higher speeds shown in the pressure distributions is an indication of separation of the flow and, consequently, large pressure drags are to be expected. Pressure-drag coefficients for the NACA 16-025 and the NACA 16-040 airfoils were obtained by combining the drag components of the normal-force coefficient with those of the chord-force coefficient. The results are presented in figure 22 together with total-drag data on a 5-inch-chord NACA 16-115 airfoil from tests in the Langley 24-inch high-speed tunnel. The drag coefficient for the thin model is small and constant throughout most of the Mach number range. The pressure-drag coefficients for the thicker models are considerably higher in

the low Mach number range because of severe separation effects; these coefficients increase rapidly at the higher Mach numbers because of the compression shock losses and increased separation losses which occur as a result of the lower critical Mach number of the thicker sections. (See figs. 3 to 10 and 22.) A comparison of the data for the several angles of attack of the NACA 16-025 airfoil shows that the drag coefficient for this model is comparatively insensitive to angle of attack in the lower Mach number range; at higher speeds the drag is markedly affected by angle-of-attack variations. In the Mach number range where a large force break is observed in the section normal-force curve (fig. 18) for the NACA 16-040 airfoil at -2°, the drag curve (fig. 22) has a similar jog. This jog can be attributed to the peculiar separation phenomena which influenced the normal-force characteristics.

Drag results were not obtained to show the effect of the variation of the location of the maximum thickness, because these effects are known to be of less importance than the effects of the large thickness changes studied. Drag data are presented primarily to show the effect of variations in the maximum thickness of the airfoil. In order to illustrate these drag variations better, the data have been recomputed on the basis of frontal area. These data (fig. 23) illustrate that the drag of the NACA 16-040 airfoil can be decreased more than 90 percent at a Mach number of 0.69 by using an NACA 16-015 airfoil of the same maximum thickness. It thus appears that the best method of reducing the propeller-shank drag is to reduce the thickness-to-chord ratio of the propeller-shank section to a value insuring favorable flow characteristics.

CONCLUSIONS

Tests to determine the effects of compressibility on the air flow and force characteristics of thick airfoil sections in a Mach number range comparable to a range of flight values for propeller-shank sections indicated that:

1. At Mach numbers approximately 0.05 above the critical value for thick airfoils, a speed region was reached in which the flow oscillated rapidly. In cases in which serious flow oscillations occurred, the flow was improved considerably by fixing transition on both surfaces of the airfoil.

2. Improvement in section characteristics may be expected from moving the maximum-thickness location from 0.3 to 0.5 chord due to drag decreases caused by the increase in critical Mach number and by the narrowing of the separated wake, particularly at supercritical speeds.

3. Relatively large improvement in section characteristics resulted from decreasing the maximum thickness of the 16-series

sections from 40 percent chord to 15 percent chord. The pressure-drag coefficient based on model thickness was reduced by as much as 90 percent at a Mach number of 0.69.

Langley Memorial Aeronautical Laboratory
National Advisory Committee for Aeronautics
Langley Field, Va., March 8, 1948

REFERENCES

1. Stack, John, and von Doenhoff, Albert E.: Tests of 16 Related Airfoils at High Speeds. NACA Rep. No. 492, 1934.

2. Stack, John: Tests of Airfoils Designed to Delay the Compressibility Burble. NACA Rep. No. 763, 1943.

3. Stack, John, Lindsey, W. F., and Littell, Robert E.: The Compressibility Burble and the Effect of Compressibility on Pressures and Forces Acting on an Airfoil. NACA Rep. No. 646, 1938.

4. Byrne, Robert W.: Experimental Constriction Effects in High-Speed Wind Tunnels. NACA ACR No. L4L07a, 1944.

5. Allen, H. Julian, and Vincenti, Walter G.: The Wall Interference in a Two-Dimensional-Flow Wind Tunnel with Consideration of the Effect of Compressibility. NACA Rep. No. 782, 1944.

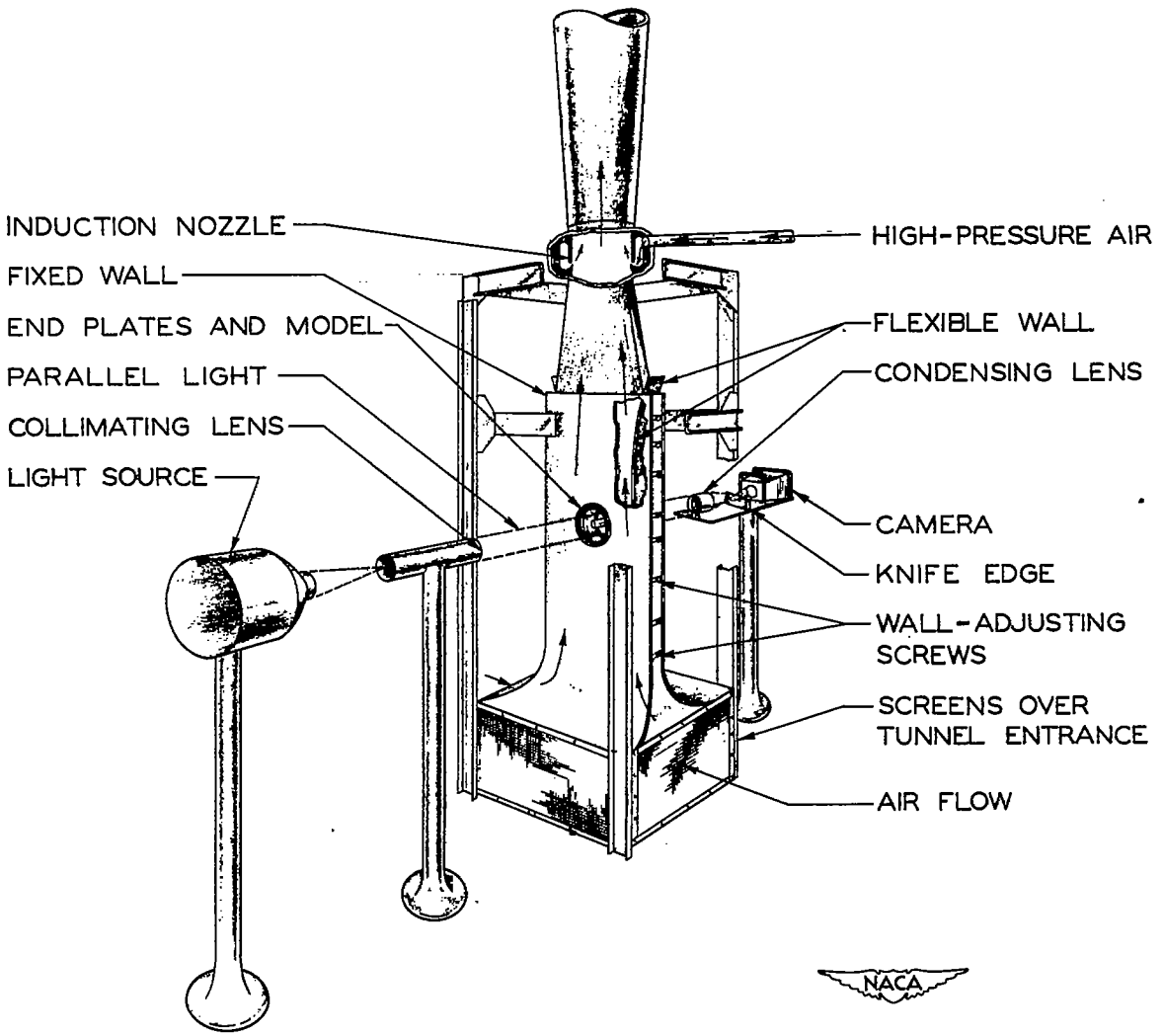

FIGURE 1.- SCHEMATIC DIAGRAM OF LANGLEY RECTANGULAR HIGH-SPEED TUNNEL AND SCHLIEREN APPARATUS.

Figure 2 .- Profiles of airfoils tested in the Langley rectangular high-speed tunnel.

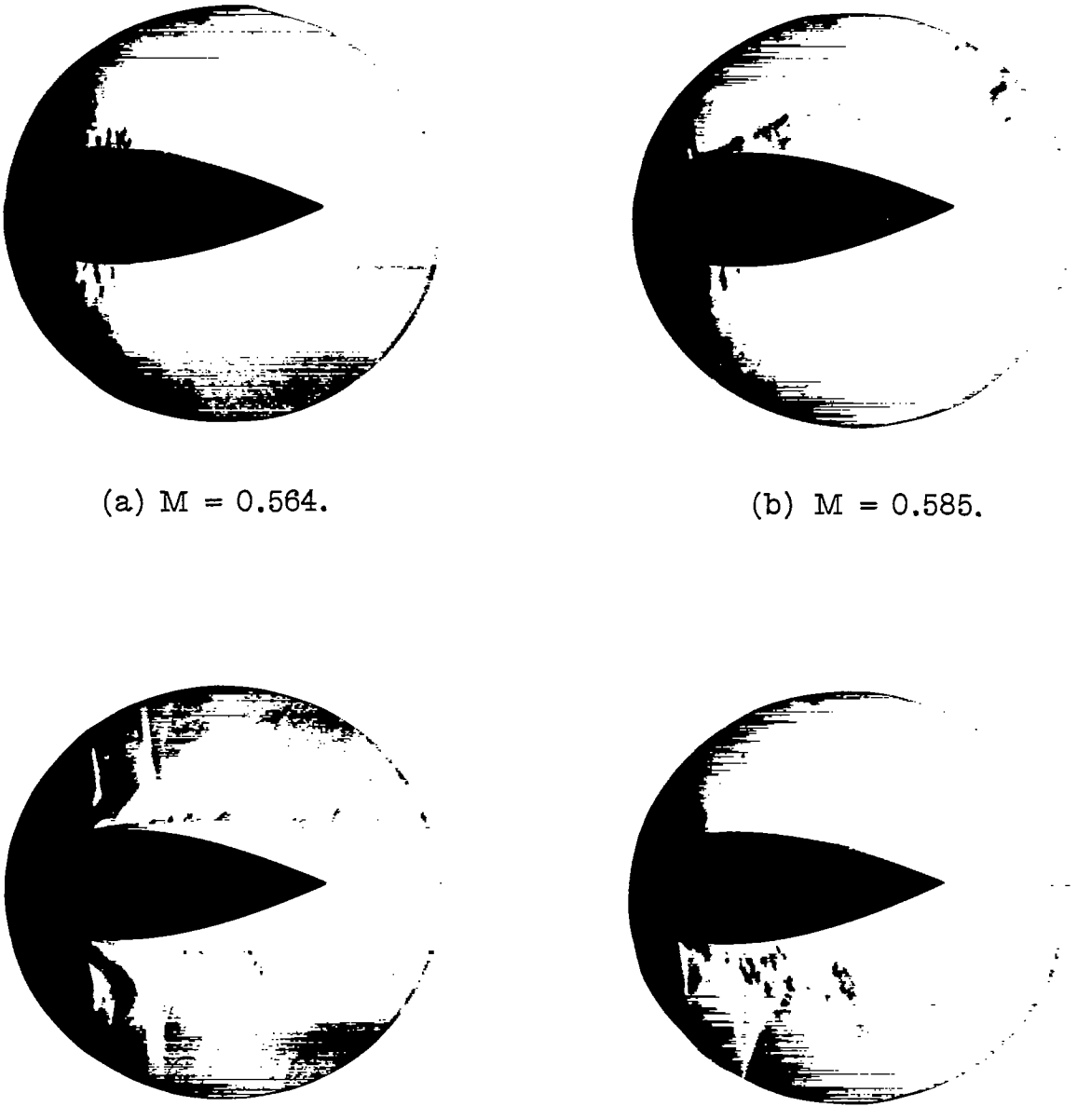

(a) M = 0.564.

(b) M = 0.585.

(c) M = 0.609.

(d) M = 0.706.

Figure 3.- Schlieren photographs of flow over NACA 0040-63 airfoil. M_{cr} = 0.510; M_{ch} = 0.714; α = 0°.

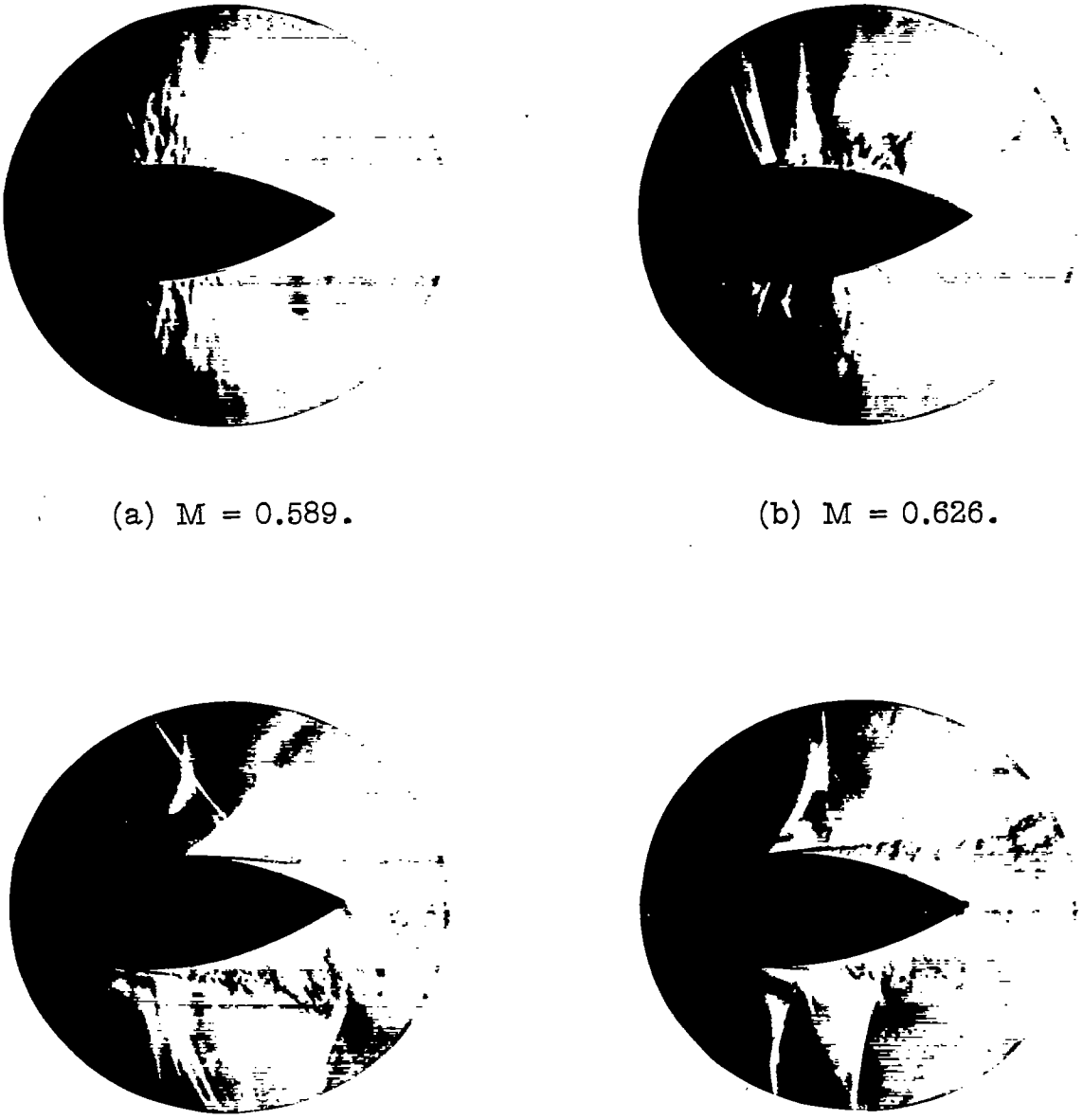

(a) M = 0.589.

(b) M = 0.626.

(c) M = 0.691.

(d) M = 0.704.

Figure 4.- Schlieren photographs of flow over NACA 0040-64 airfoil. $M_{cr} = 0.550$; $M_{ch} = 0.721$; $\alpha = 0°$.

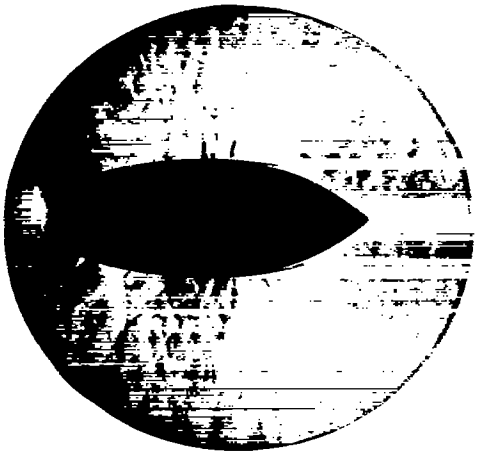

(a) M = 0.602.

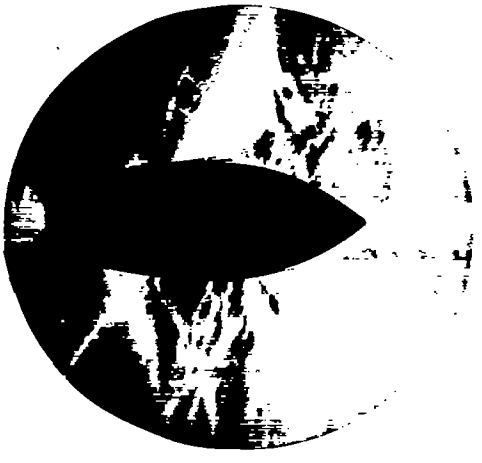

(b) M = 0.678.

(c) M = 0.707.

(d) M = 0.731.

Figure 5.- Schlieren photographs of flow over NACA 0040-65 airfoil. $M_{cr} = 0.580$; $M_{ch} = 0.731$; $\alpha = 0^{\circ}$.

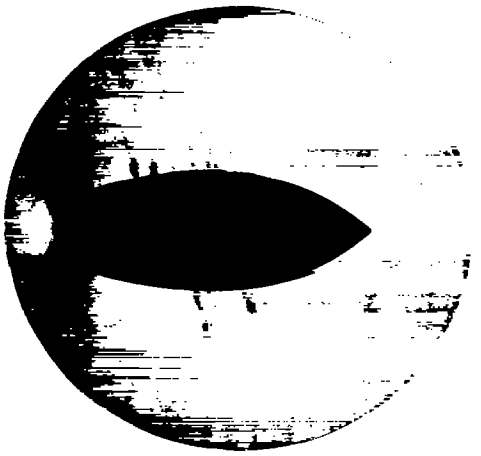

(a) M = 0.600.

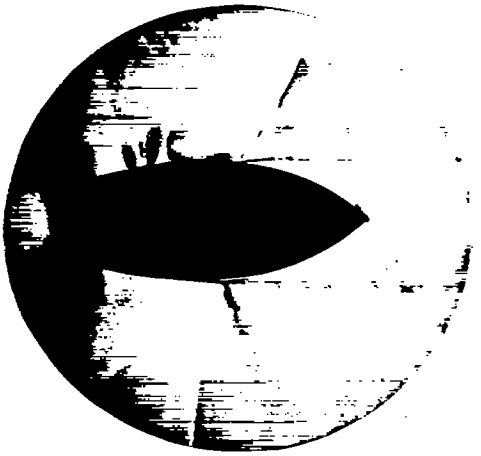

(b) M = 0.677.

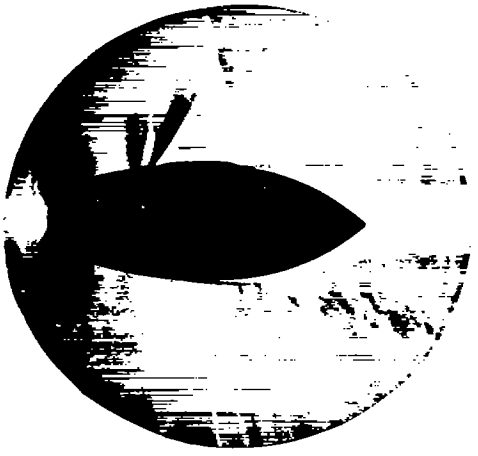

(c) M = 0.707.

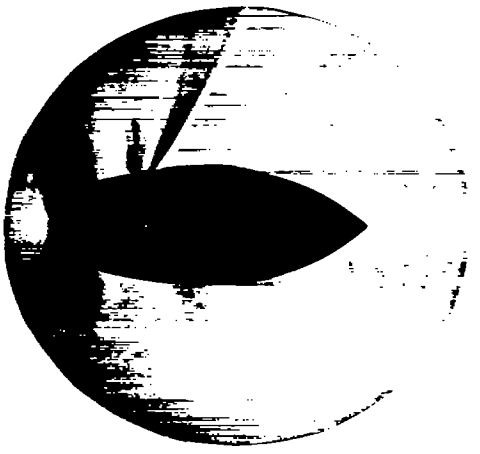

(d) M = 0.729.

Figure 6.- Schlieren photographs of flow over NACA 0040-65 airfoil with transition fixed at 0.25 chord on upper surface. M_{cr} = 0.580; M_{ch} = 0.729; $\alpha = 0^{\circ}$.

(a) M = 0.600.

(b) M = 0.676.

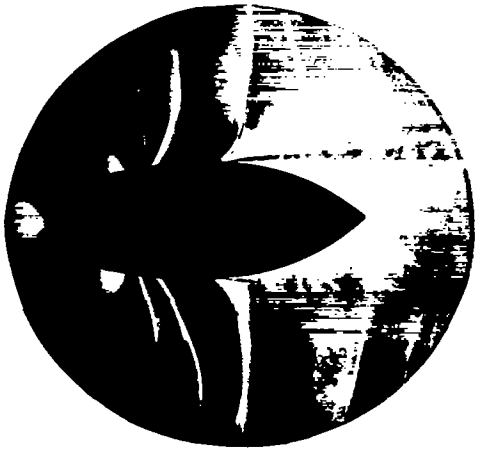

(c) M = 0.707.

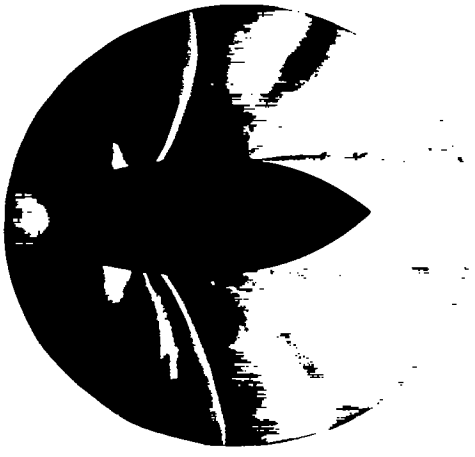

(d) M = 0.727.

Figure 7.- Schlieren photographs of flow over NACA 0040-65 airfoil with transition fixed at 0.25 chord on the upper and lower surfaces. M_{cr} = 0.580; M_{ch} = 0.727; $\alpha = 0^{\circ}$.

(a) M = 0.597.

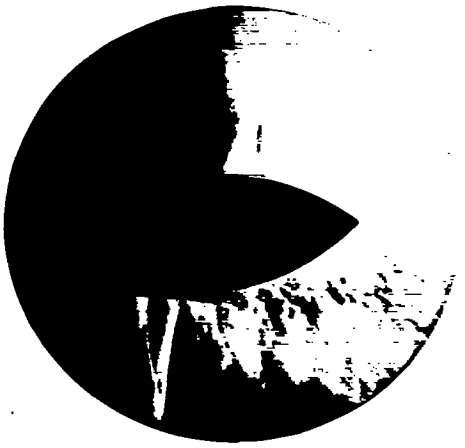

(b) M = 0.632.

(c) M = 0.711.

(d) M = 0.723.

Figure 8.- Schlieren photographs of flow over NACA 16-040 airfoil. $M_{cr} = 0.575$; $M_{ch} = 0.729$; $\alpha = 0^{\circ}$.

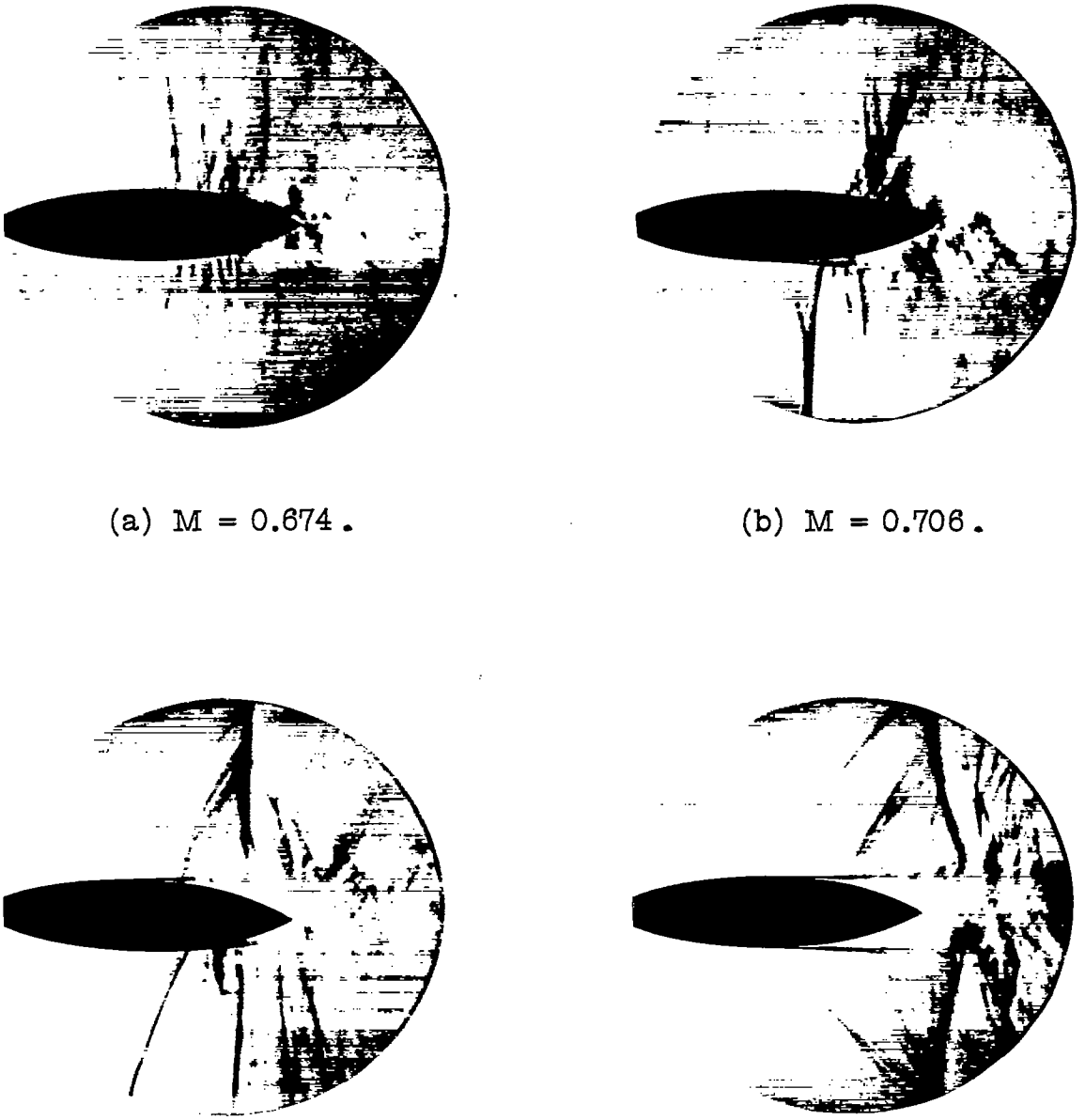

(a) M = 0.674.

(b) M = 0.706.

(c) M = 0.758.

(d) M = 0.776.

Figure 9.- Schlieren photographs of flow over NACA 16-025 airfoil. $M_{cr} = 0.657$; $M_{ch} = 0.787$; $\alpha = 0°$.

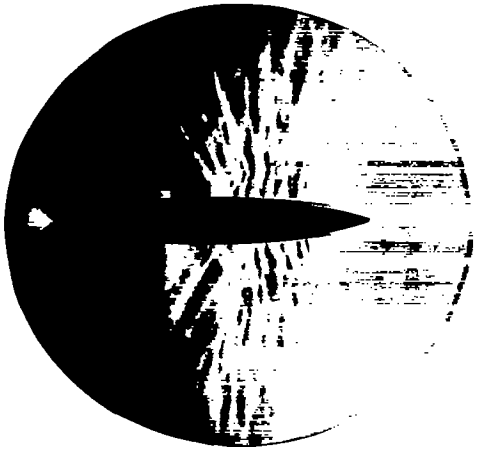

(a) M = 0.756.

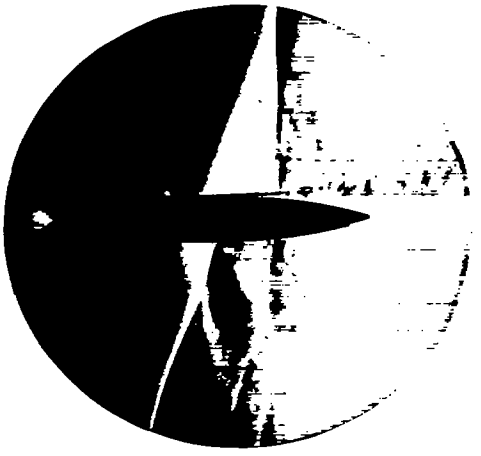

(b) M = 0.788.

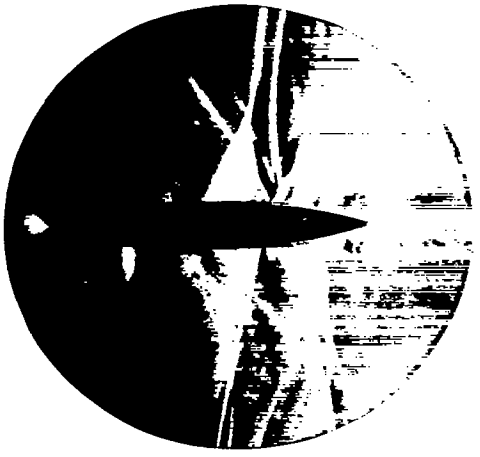

(c) M = 0.808.

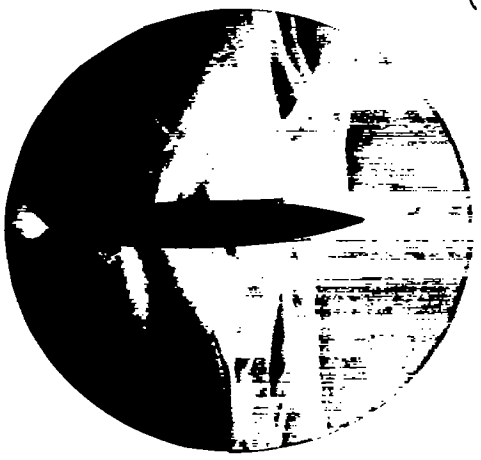

(d) M = 0.826.

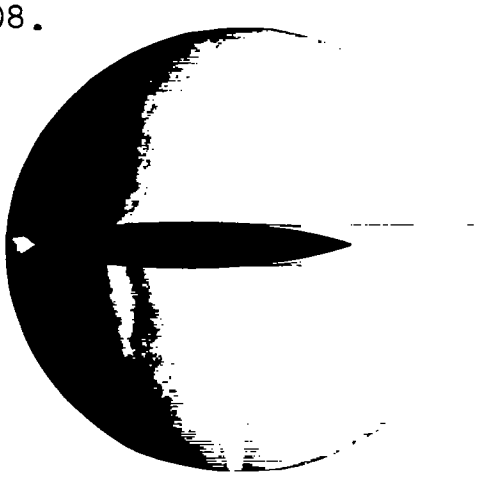

(e) M = 0.838.

Figure 10.- Schlieren photographs of flow over NACA 16-015 airfoil. M_{cr} = 0.730; M_{ch} = 0.847; α = 0°.

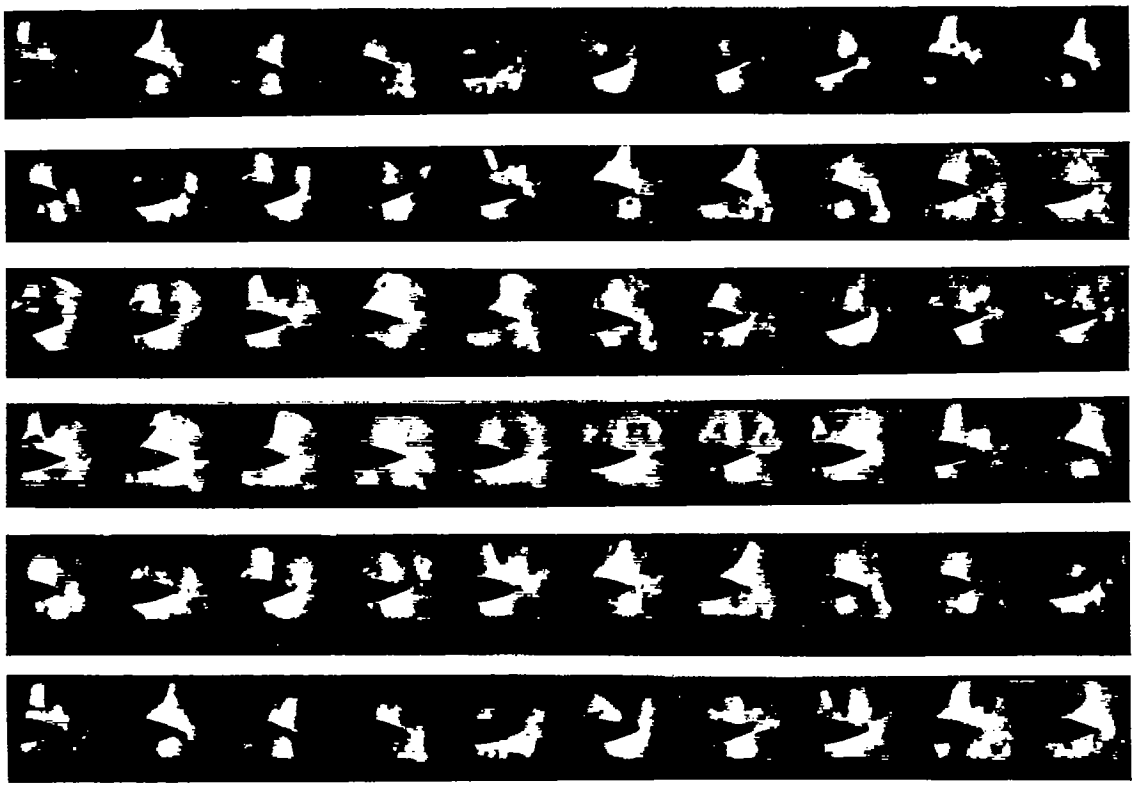

Figure 11.- Continuous motion-picture sequence illustrating oscillating flow. Camera speed, 2060 frames per second; NACA 0040-63 airfoil; $M = 0.63$; $M_{cr} = 0.510$; $M_{ch} = 0.714$; $\alpha = 0°$.

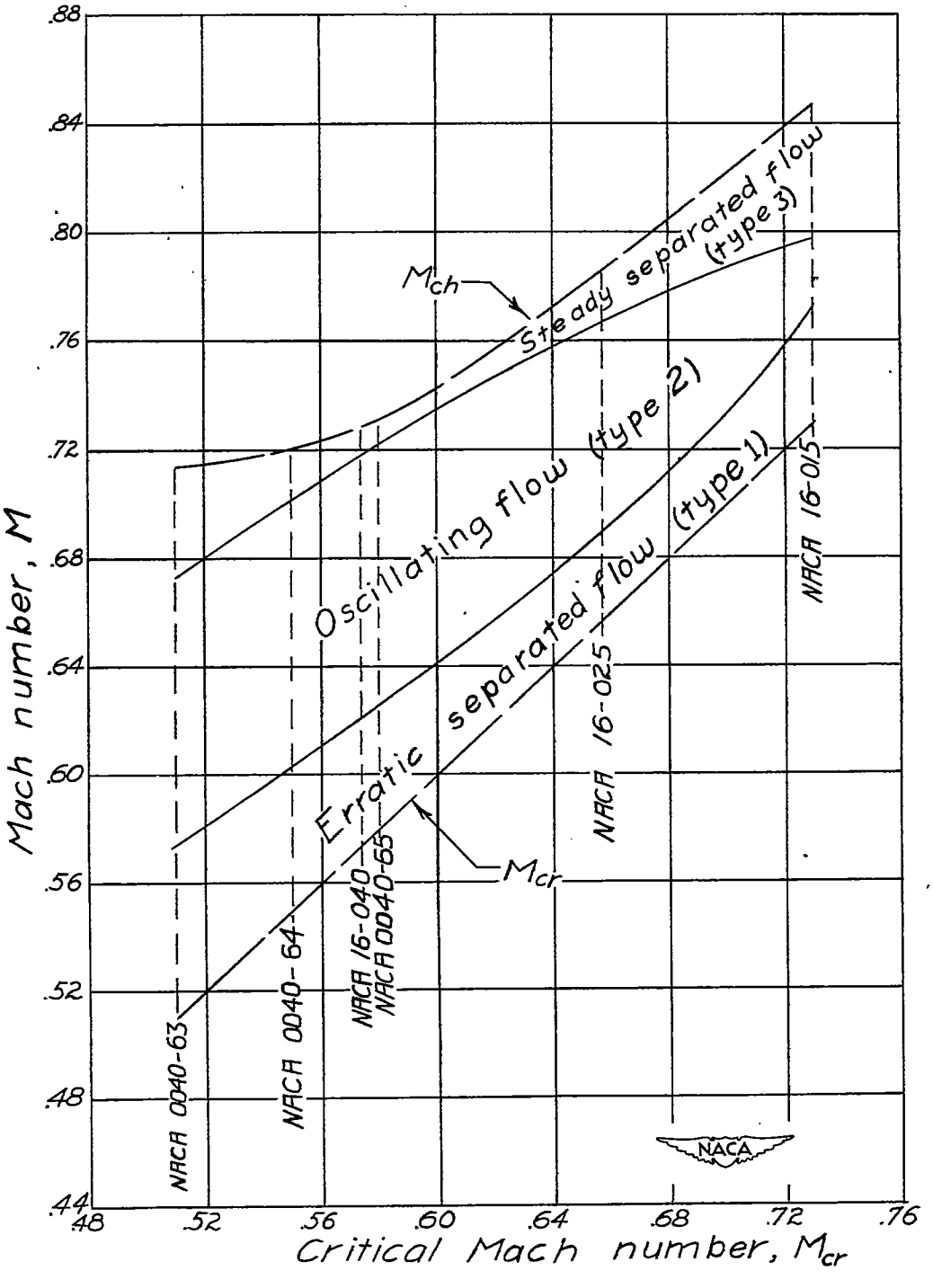

Figure 12.- Supercritical flow boundaries for NACA airfoils tested. $\alpha = 0°$.

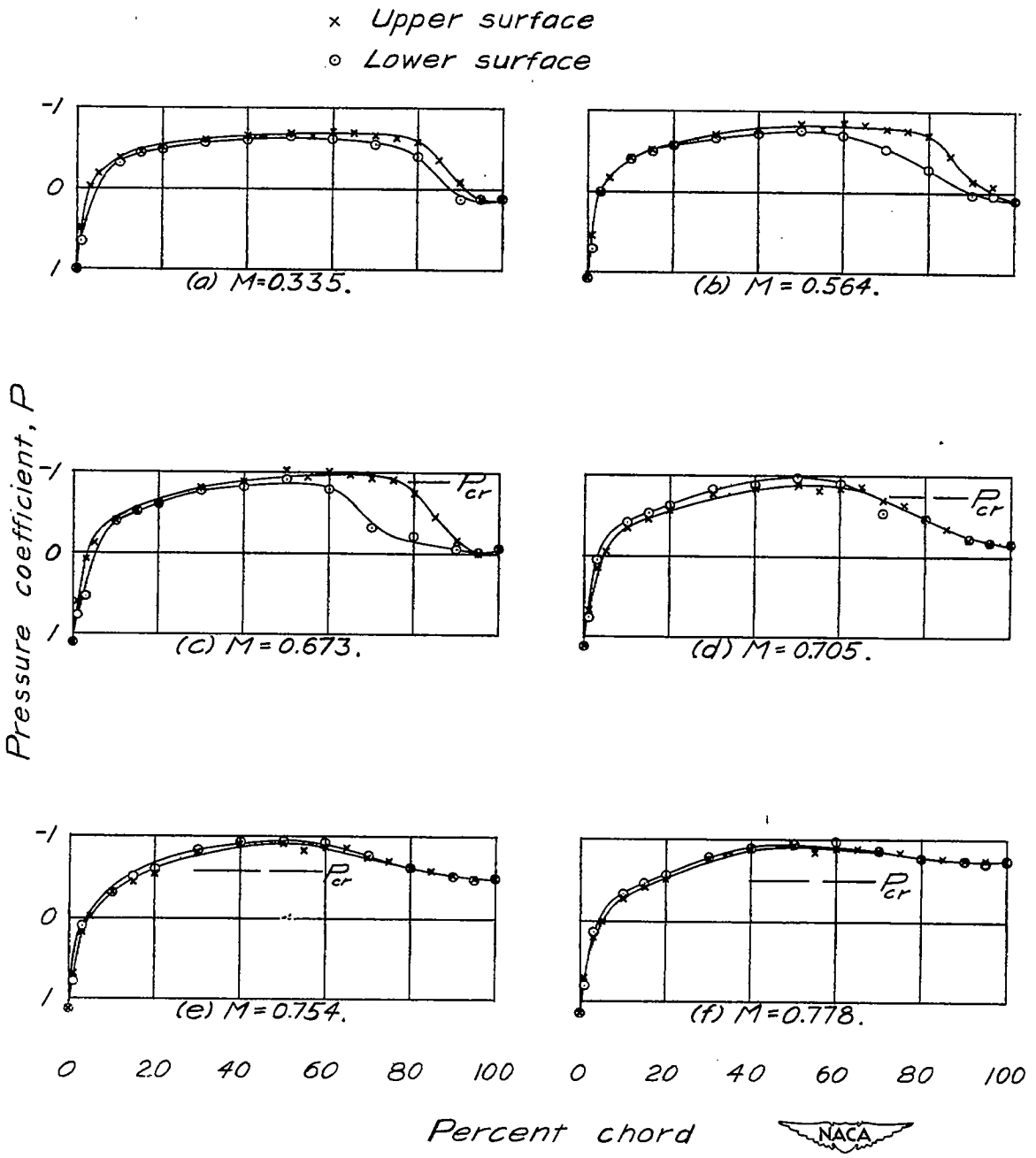

Figure 13.— Pressure distribution for an NACA 16-025 airfoil. M_{cr}=0.657; M_{ch}=0.787 ; $\alpha = 0°$.

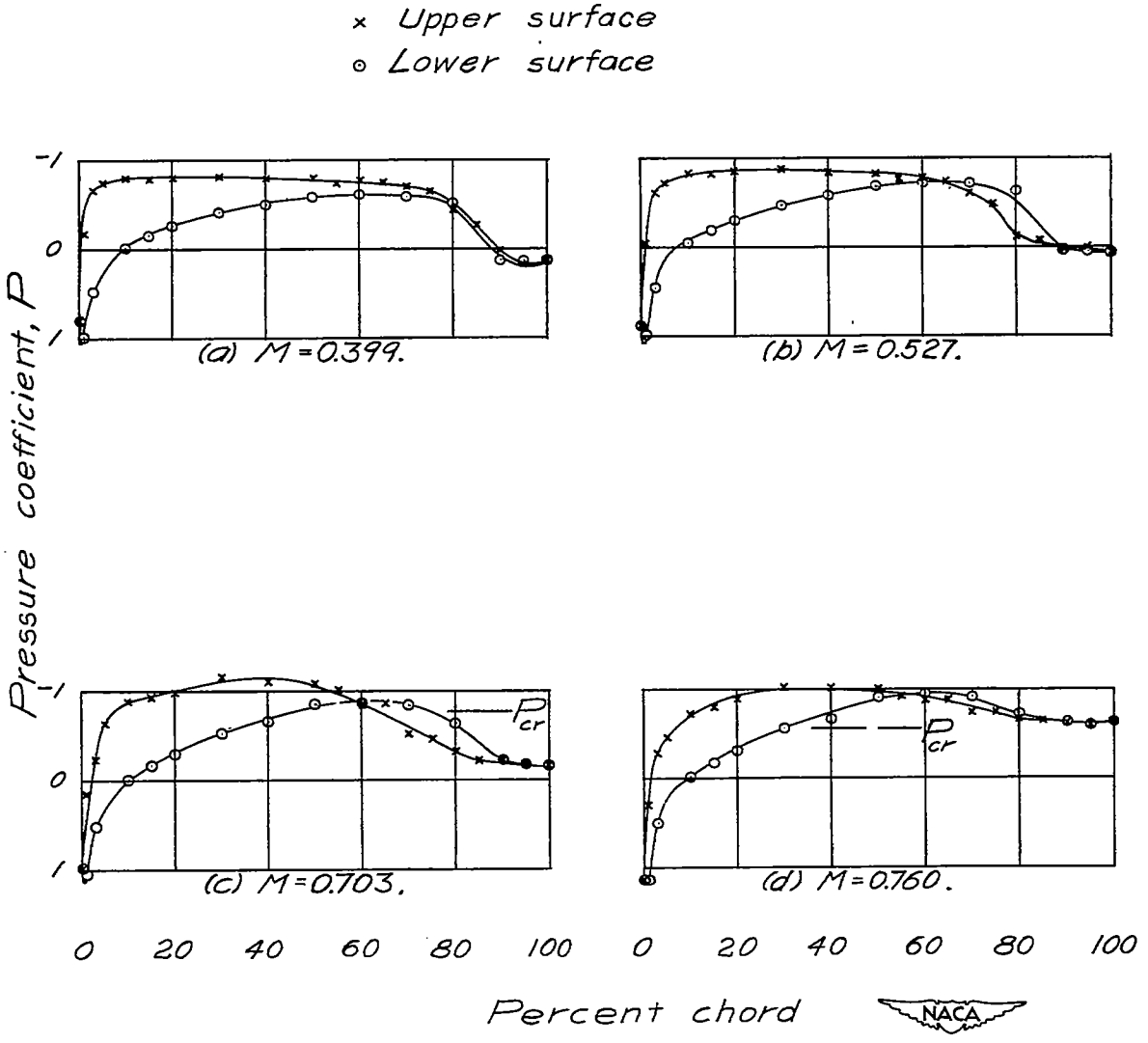

Figure 14. — Pressure distribution for an NACA 16-025 airfoil. $M_{cr} = 0.646$; $M_{ch} = 0.785$; $\alpha = 4°$.

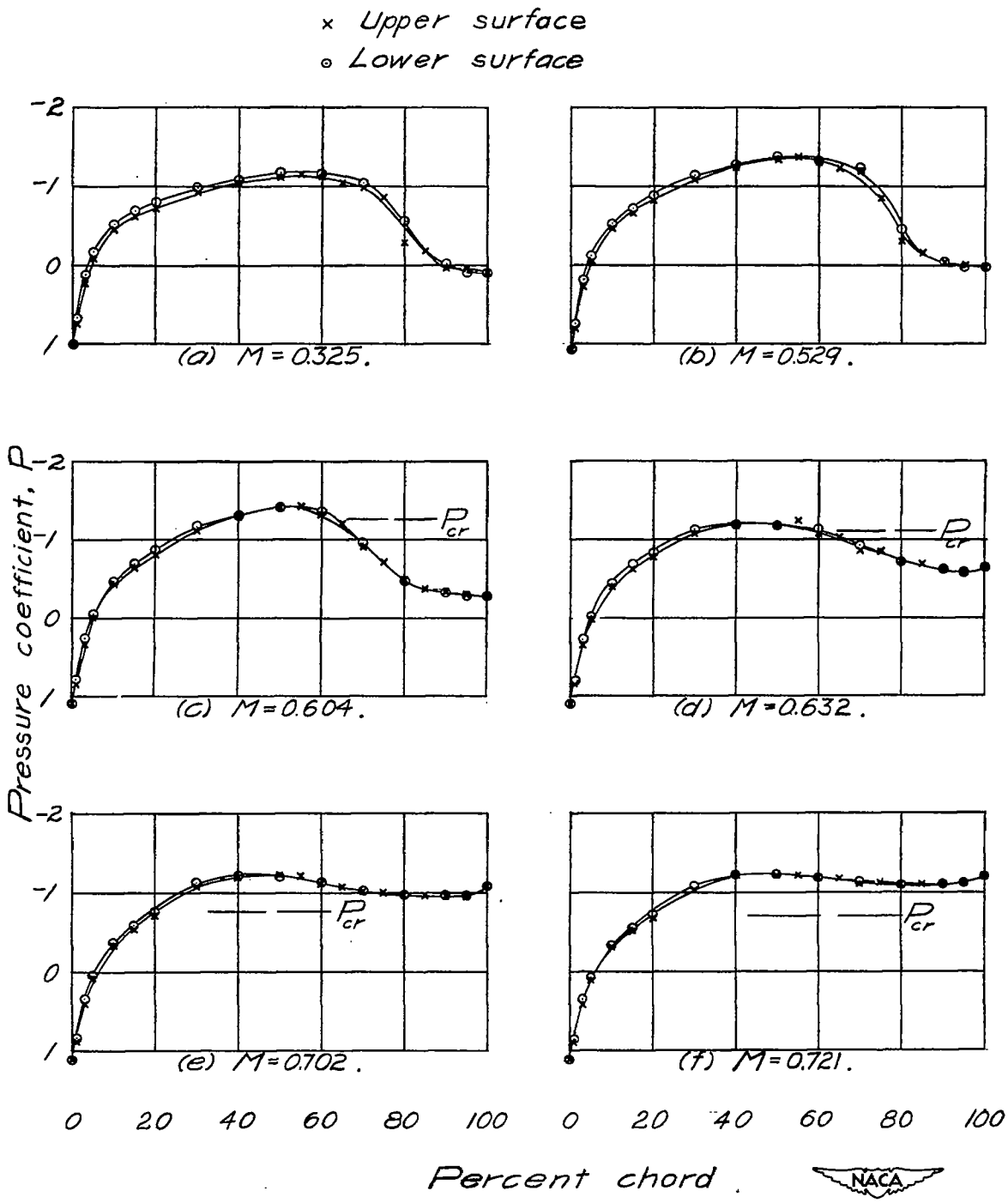

Figure 15.— Pressure distribution for an NACA 16-040 airfoil. $M_{cr} = 0.575$; $M_{ch} = 0.729$; $\alpha = 0°$.

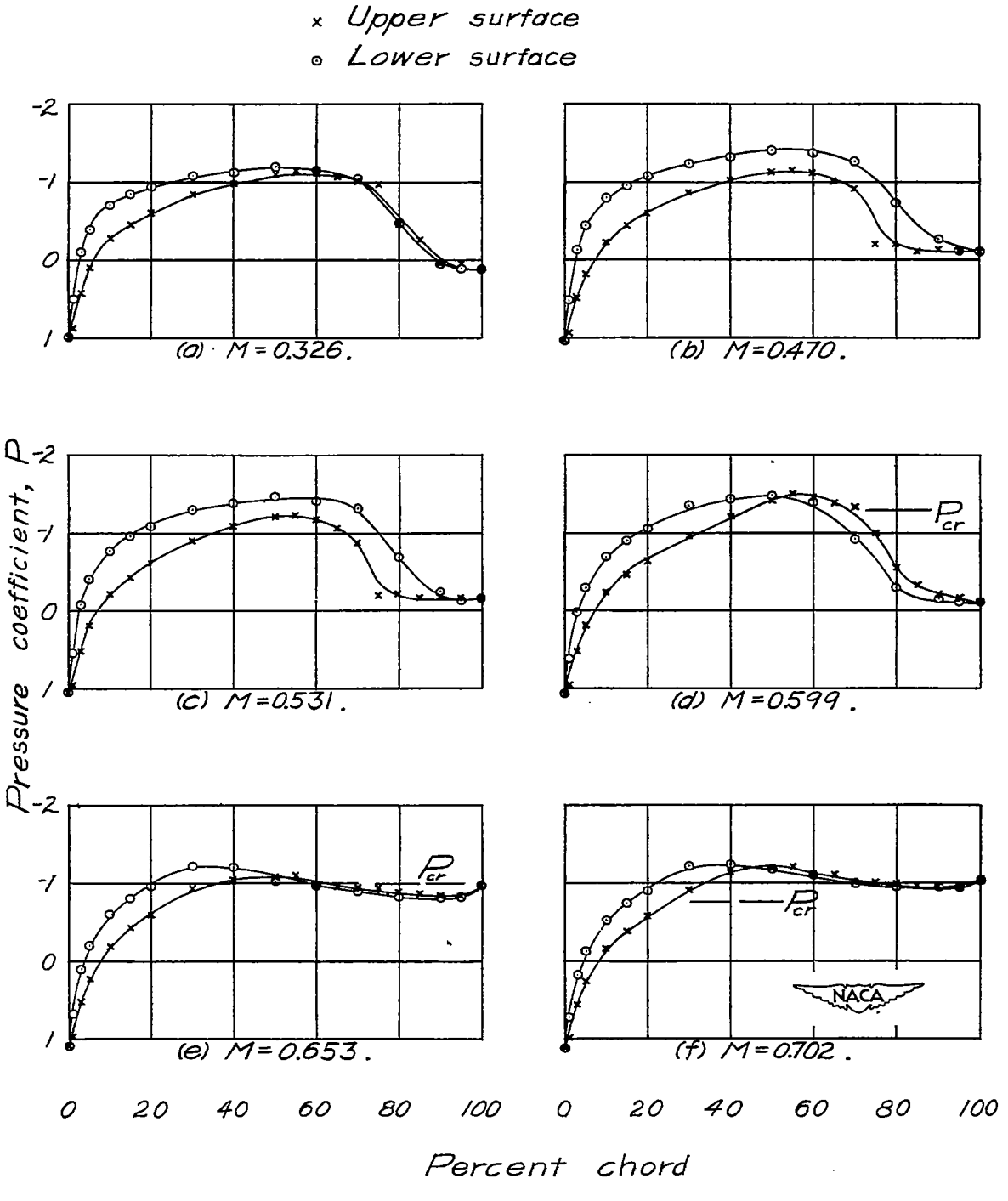

Figure 16.— Pressure distribution for an NACA 16-040 airfoil. M_{cr}=0.564; M_{ch}=0.727; α=-2°.

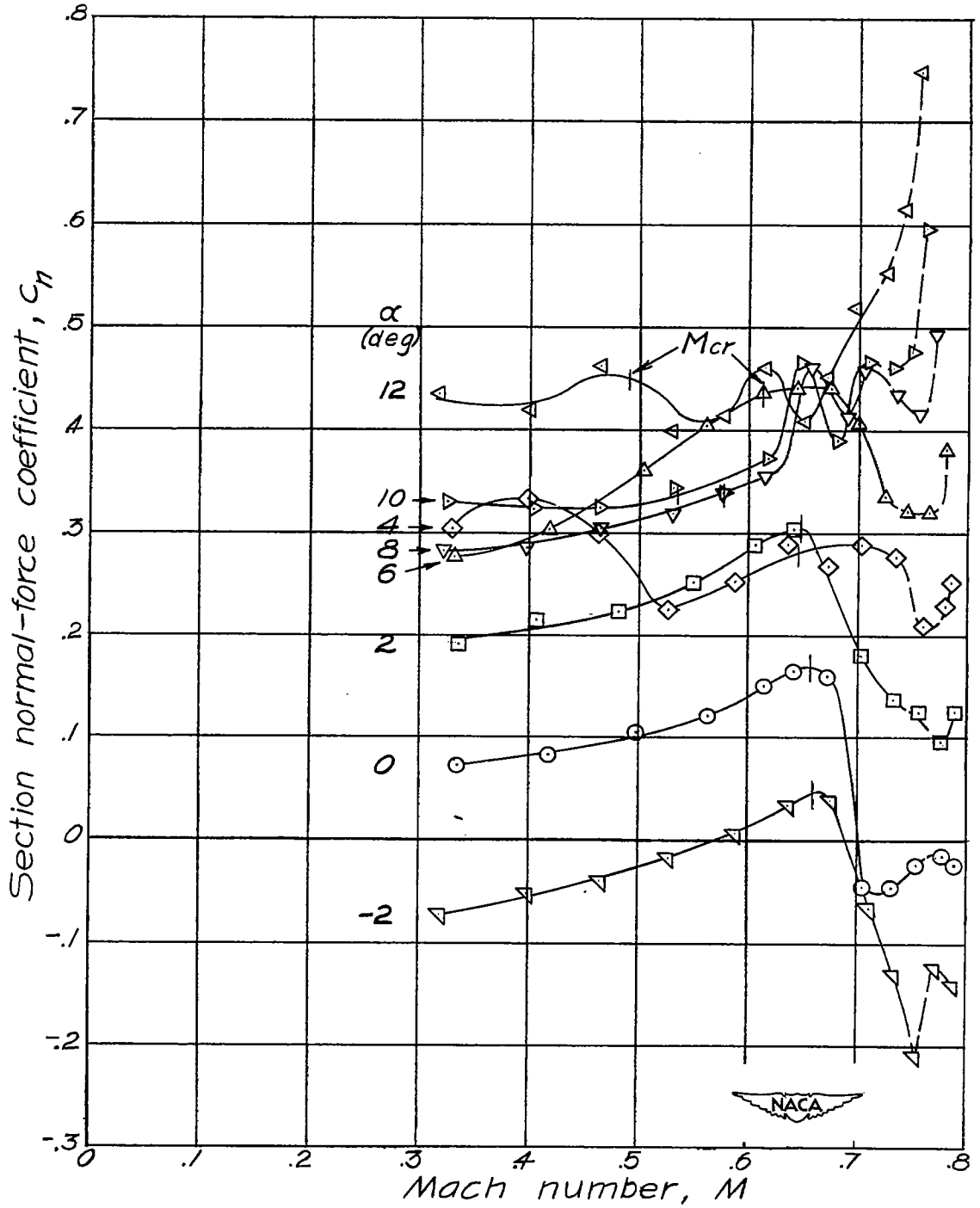

Figure 17.- Variation of section normal-force coefficient with Mach number. NACA 16-025 airfoil.

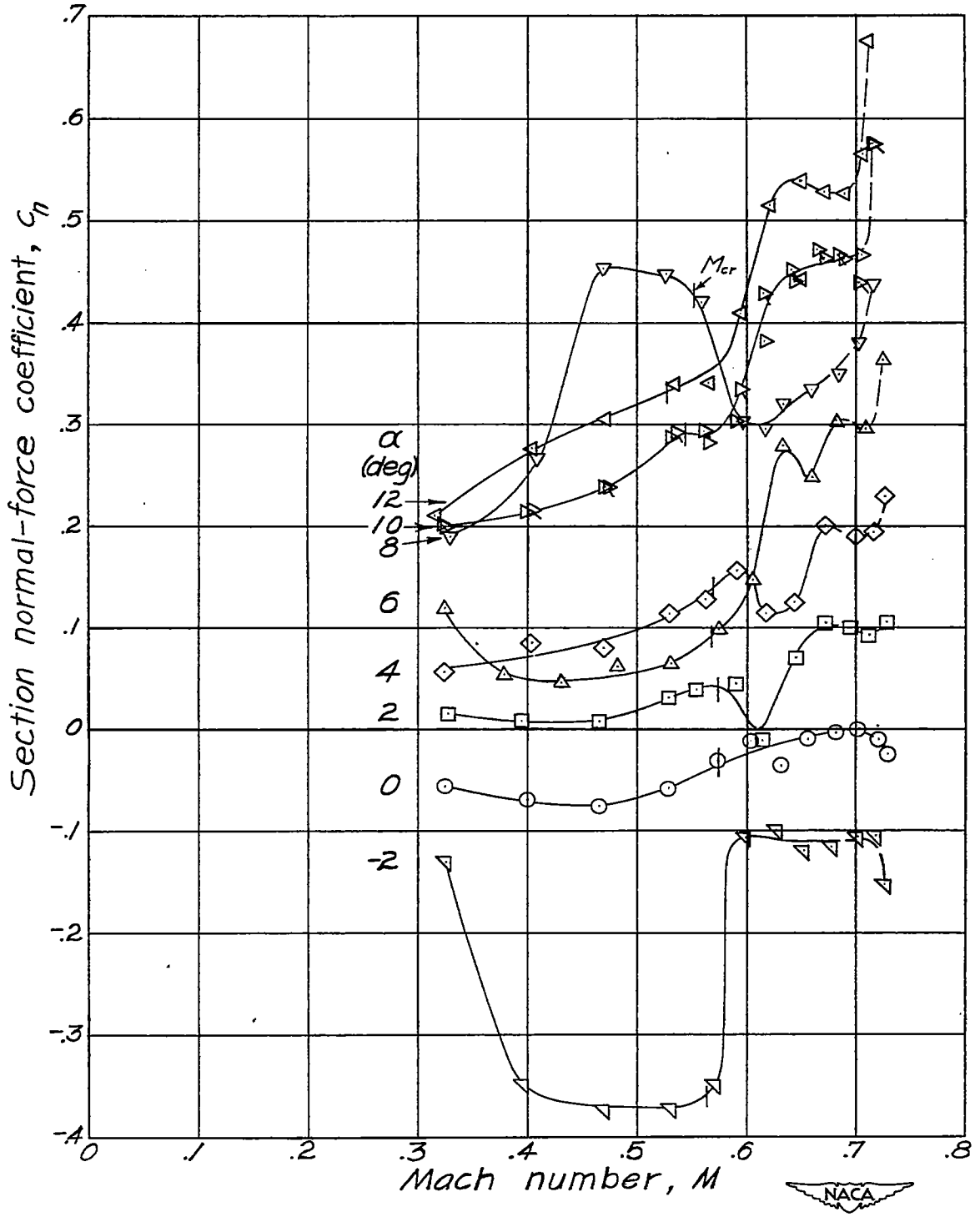

Figure 18.— Variation of section normal-force coefficient with Mach number. NACA 16-040 airfoil.

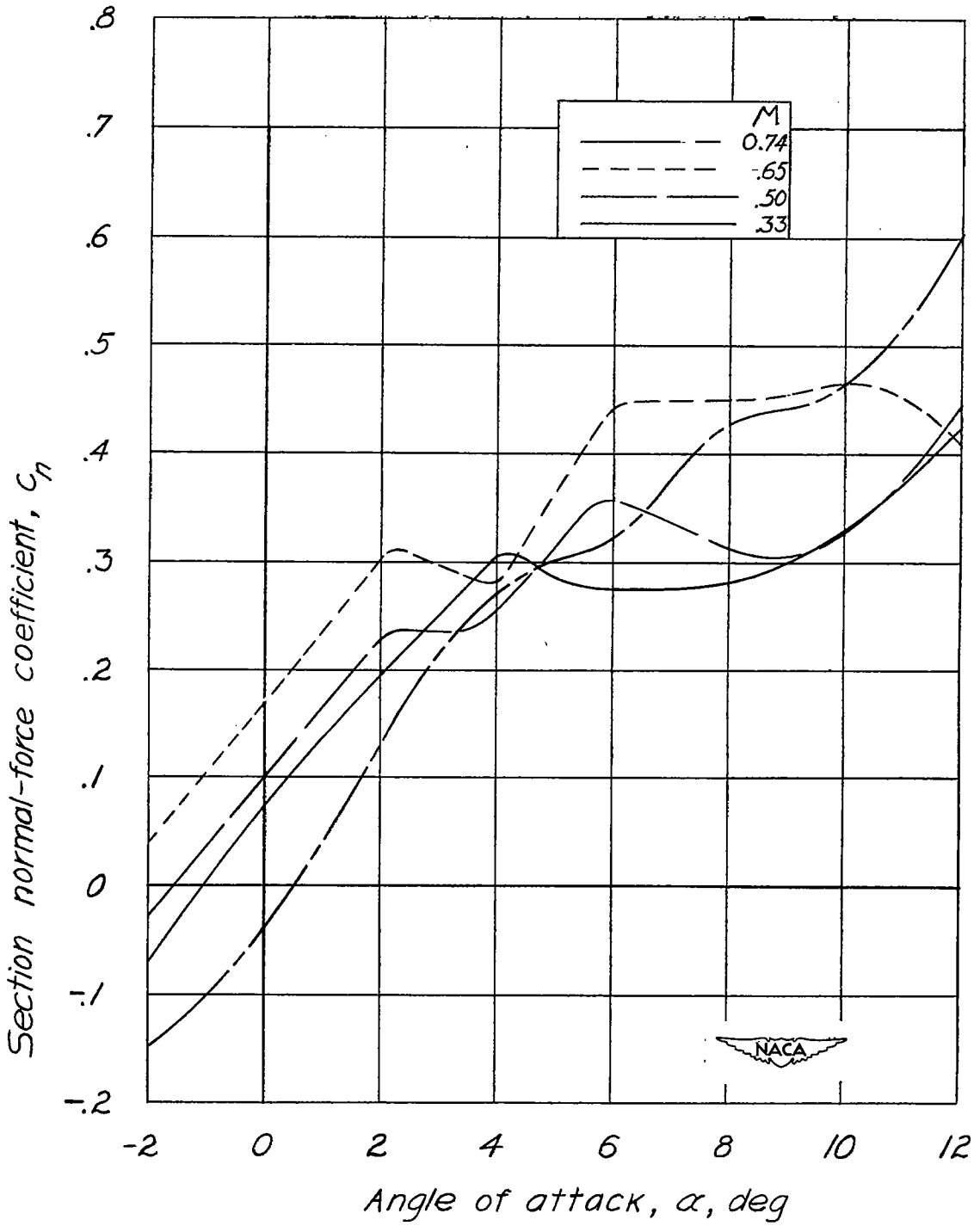

Figure 19.- Variation of section normal-force coefficient with angle of attack. NACA 16-025 airfoil.

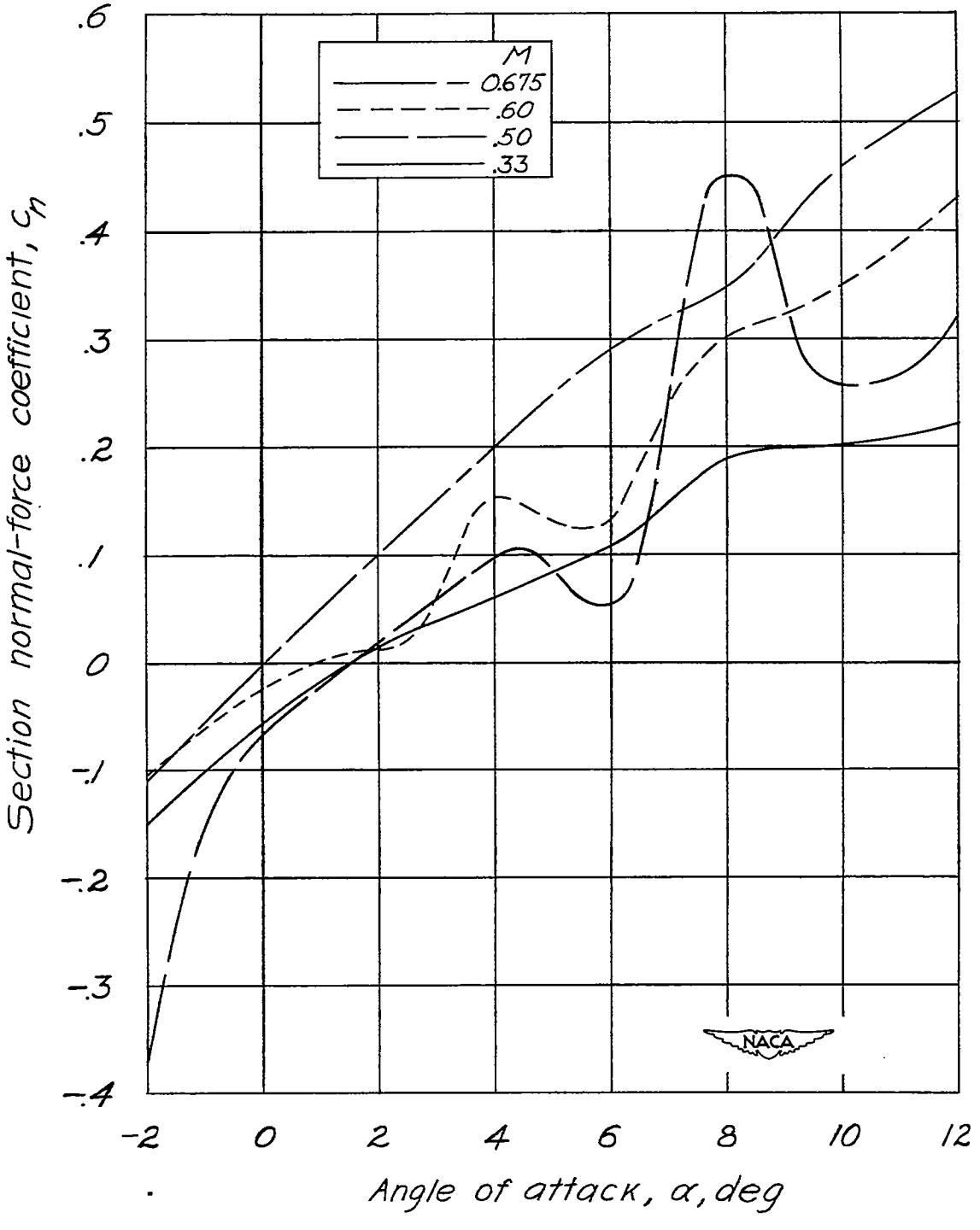

Figure 20.– Variation of section normal-force coefficient with angle of attack. NACA 16-040 airfoil.

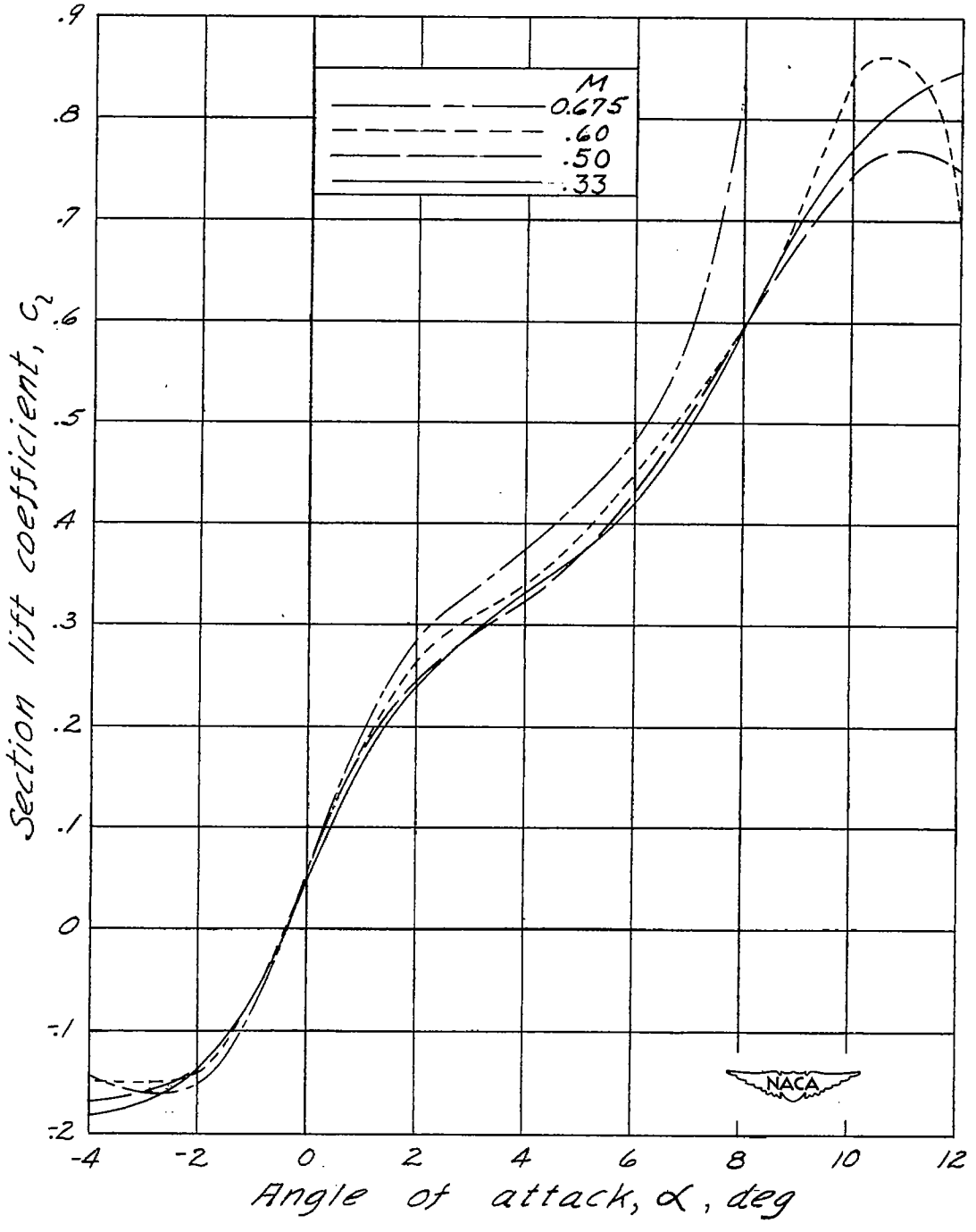

Figure 21.- Variation of section lift coefficient with angle of attack for the NACA 16-115 airfoil. Data from Langley 24-inch high-speed tunnel.

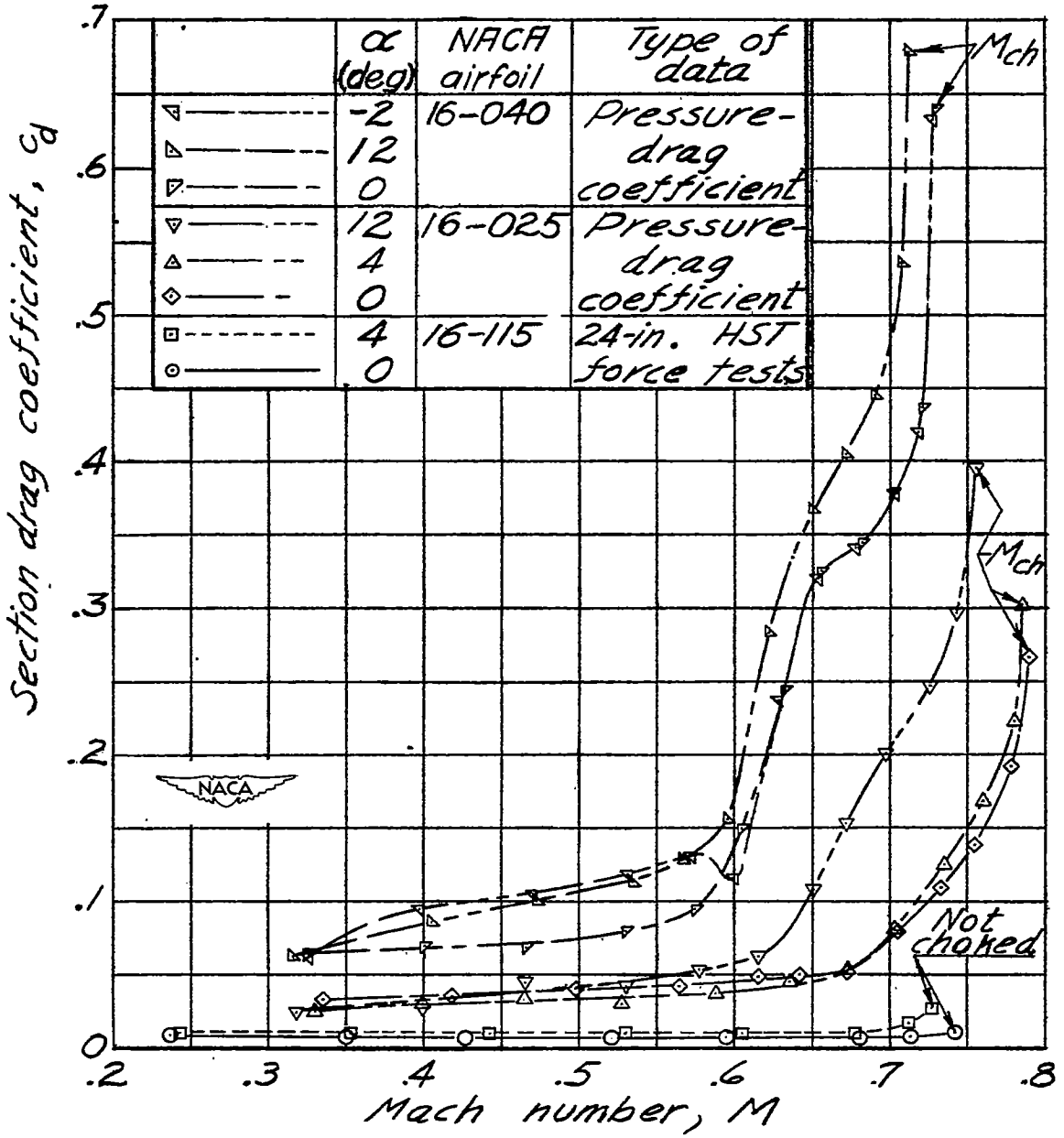

Figure 22.- Section drag characteristics for the NACA 16-040, 16-025, and 16-115 airfoils. (Langley 24-inch high-speed tunnel designated Langley 24-in. HST.)

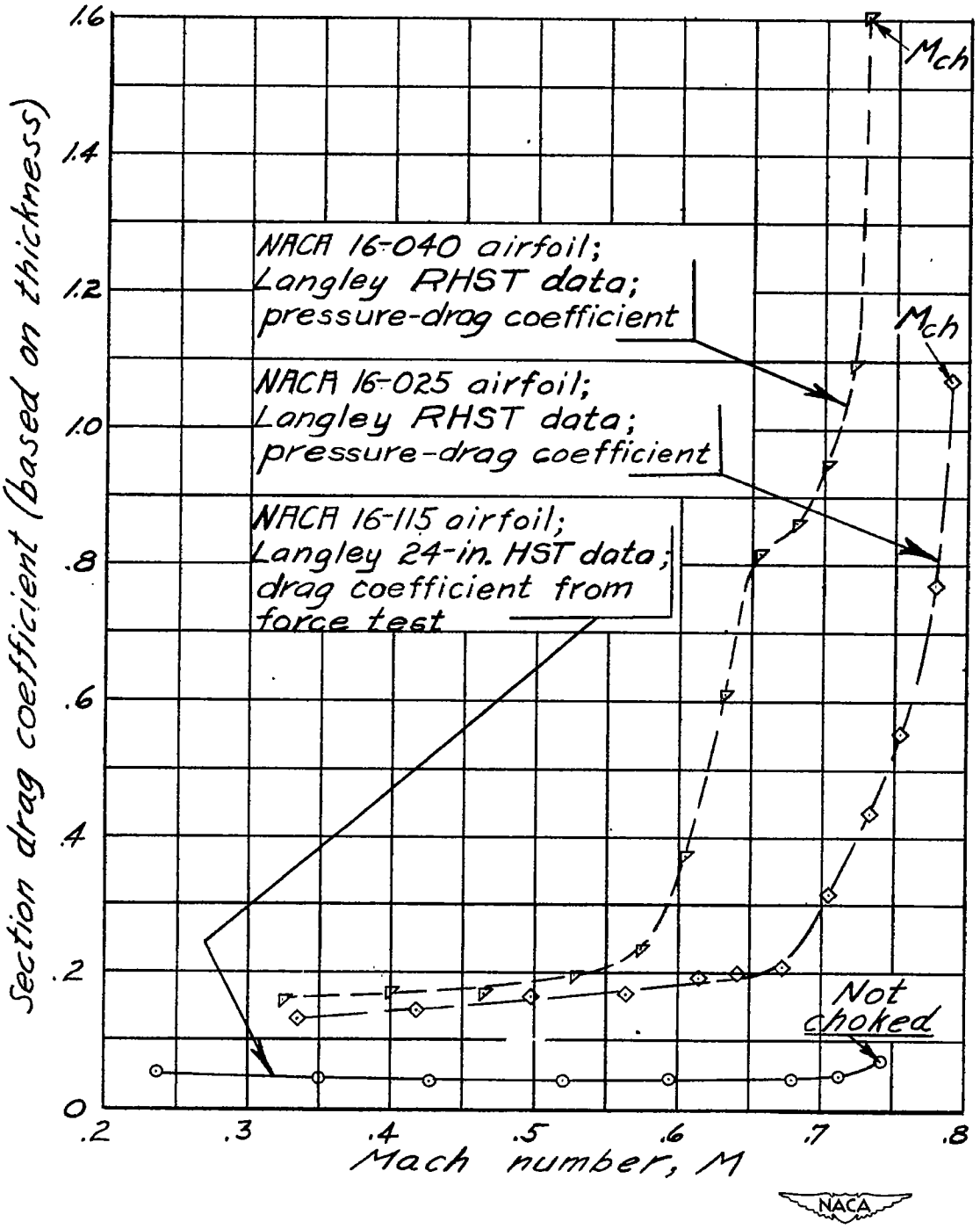

Figure 23. – Section drag characteristics (based on model thickness) for the NACA 16-040, 16-025, and 16-115 airfoils. $\alpha = 0°$. (Langley rectangular high-speed tunnel designated Langley RHST.)